PHYSICAL REVIEW D **92,** 055033 (2015)

Hidden dark matter sector, dark radiation, and the CMB

Zackaria Chacko,[1] Yanou Cui,[1,2] Sungwoo Hong,[1] and Takemichi Okui[3]

[1]*Maryland Center for Fundamental Physics, Department of Physics, University of Maryland, College Park, Maryland 20742, USA*

[2]*Perimeter Institute for Theoretical Physics, Waterloo, Ontario N2L 2Y5, Canada*

[3]*Department of Physics, Florida State University, Tallahassee, Florida 32306, USA*

(Received 23 June 2015; published 28 September 2015)

We consider theories where dark matter is composed of a thermal relic of weak scale mass, whose couplings to the standard model (SM) are however too small to give rise to the observed abundance. Instead, the abundance is set by annihilation to light hidden sector states that carry no charges under the SM gauge interactions. In such a scenario the constraints from direct and indirect detection, and from collider searches for dark matter, can easily be satisfied. The masses of such light hidden states can be protected by symmetry if they are Nambu-Goldstone bosons, fermions, or gauge bosons. These states can then contribute to the cosmic energy density as dark radiation, leading to observable signals in the cosmic microwave background (CMB). Furthermore, depending on whether or not the light hidden sector states self-interact, the fraction of the total energy density that free-streams is either decreased or increased, leading to characteristic effects on both the scalar and tensor components of the CMB anisotropy that allows these two cases to be distinguished. The magnitude of these signals depends on the number of light degrees of freedom in the hidden sector, and on the temperature at which it kinetically decouples from the SM. We consider a simple model that realizes this scenario, based on a framework in which the SM and hidden sector are initially in thermal equilibrium through the Higgs portal, and show that the resulting signals are compatible with recent Planck results, while large enough to be detected in upcoming experiments such as CMBPol and CMB Stage-IV. Invisible decays of the Higgs into hidden sector states at colliders can offer a complementary probe of this model.

DOI: 10.1103/PhysRevD.92.055033 PACS numbers: 95.35.+d, 12.60.-i, 98.80.-k

I. INTRODUCTION

In the last two decades, with the advent of precision cosmology, it has become clear that some form of nonluminous dark matter (DM) contributes more than 20% of the total energy density of the universe [1]. Although it is known that the particles of which DM is composed lie outside the SM of particle physics, their precise nature remains to be understood.

In the absence of a detailed understanding about the properties of dark matter, many different candidates have been put forward. A large class of well-motivated theories are based on the "weakly interacting massive particle" (WIMP) paradigm. In its simplest incarnation, this scenario involves a particle of weak scale mass, the WIMP, that has interactions of weak scale strength with the SM fields. This class of theories possesses the very attractive feature that the WIMPs that survive after their annihilation into SM particles freezes out naturally tend to have a relic abundance that is in good agreement with observations [2,3].

In this conventional scenario, the WIMP must have interactions of weak scale strength with the SM fields. Several different types of DM experiments are searching for evidence of such interactions. These include direct detection experiments that are looking for the recoils of nuclei after being impacted by a DM particle, indirect detection experiments that seek to observe the products of DM annihilation, and collider experiments such as the Large Hadron Collider (LHC) that seek to produce DM. To date, there has been no compelling evidence for the existence of such interactions, and the experimental limits now exclude a significant part of the preferred parameter space for many WIMP DM candidates [4–8].

With the simplest realizations of the WIMP paradigm beginning to come under strain, several ideas have been put forward to explain the absence of a signal in these experiments. Among the hypotheses that have been advanced are that the DM candidate scatters inelastically [9,10], is leptophilic [11–13], or interacts preferentially with heavier quark flavors [14–18]. An alternative proposal that has attracted interest [19–22] is the idea that, while DM is indeed composed of WIMPs, their couplings to the SM fields are suppressed, and too small to yield the observed abundance. Instead, the DM candidate possesses interactions of weak scale strength with a new hidden sector that carries no charge under the SM gauge interactions, and its relic abundance is set by its annihilation into these states. Such a scenario can naturally account for the observed abundance of DM, while explaining the absence of any signal in experiments.

It is not difficult to envisage scenarios where the DM candidate naturally has weak scale mass and interactions of

weak scale strength with a hidden sector. For example, in supersymmetric theories, both the weak scale and the scales in the hidden sector could be set by the scale of supersymmetry breaking. Similarly, in extra dimensional Randall-Sundrum constructions, both the Higgs and the hidden sector states could be localized to the infrared brane. In such a scenario the scales in the hidden sector would again naturally be of order the weak scale. Therefore, provided the SM and hidden sectors are in thermal equilibrium at or above the weak scale, so that their temperatures at freeze-out are not very different, this framework can naturally explain the observed abundance of DM while remaining consistent with all experimental constraints.

The existence of a hidden sector into which DM annihilates can potentially be tested by experiments. The nature of the signals depends on the masses of the particles in the hidden sector, and on their couplings to SM states. If all the particles in the hidden sector have masses above an eV, and the temperature of this sector is comparable to that of the SM, we expect these states will decay or annihilate into SM particles before the CMB epoch. This is because the lightest state in the hidden sector, being massive, would otherwise contribute to the energy density in DM, violating the overclosure bounds if it is heavier than a keV, and coming into conflict with the cosmological constraints on a warm subcomponent of DM if it is lighter than a keV. Such a scenario therefore implies the existence of couplings between the hidden sector states and the SM that can potentially be tested in experiments, as in the scenarios of exciting DM [19,23], secluded DM [20] and boosted DM [24,25]. If instead, some or all of the states in the hidden sector have masses below an eV, they would be expected to constitute a significant component of the energy density of the universe both before and during the epoch of matter-radiation equality, potentially leading to observable signals in the CMB [21,22,26–31]. The simplest possibility is that these states, if present, are massless, and constitute dark radiation (DR) at present times, thereby obviating the need for any other mass scales in the theory. It is this scenario, and the associated signals, that we will focus on in this paper.[1]

The presence of these new light particles implies the existence of additional structure in the theory, if the scenario is to be natural. There are three known symmetries that can prevent masses from being generated for a massless particle: a shift symmetry for a spin-0 Nambu-Goldstone boson, a chiral symmetry for a spin-1/2 fermion, and a gauge symmetry for a spin-1 vector boson. DR candidates protected by these symmetries have been considered, for example, in [36,37]. These symmetries may appear individually or in combination; for example, the spectrum of light states may consist of a single Nambu-Goldstone boson, but it may also consist of spin-1/2 fermions charged under a U(1) gauge group with its associated massless spin-1 boson [38]. This latter example illustrates that the constituents of the DR need not be free, but may have interactions amongst themselves without violating the symmetries that keep them light. In general, therefore, we see that the DR can take two distinct forms:

(i) *Free DR*, which free streams during the era of acoustic oscillations, and is characterized by a mean free path $\gg H^{-1}$, where H is the Hubble constant.
(ii) *Scattering DR*, which scatters during the era of acoustic oscillations, and is characterized by a mean free path $\ll H^{-1}$.

Since the presence of DR is a robust prediction of this scenario, it is important to understand whether it can be detected, and whether we can distinguish between the two different cases of free DR and scattering DRİt is these questions that we shall be primarily concerned with in this paper. We find that, provided the hidden DM sector was in thermal equilibrium with the SM at temperatures at or above the weak scale, the contribution of the DR to the energy density during the CMB epoch is in general large enough to be detected in future experiments, such as CMBPol [39] ($\sigma_{N_{\rm eff}} = 0.044$), and eventually CMB Stage-IV [40] ($\sigma_{N_{\rm eff}} = 0.02$).

We also find that it is, in general, possible to distinguish between scenarios with free streaming DR and scattering DR. Studies of the scalar [41–43] and tensor [44,45] metric perturbations have established that the details of the CMB spectrum depend on the fraction of the energy density in radiation that is free streaming. This ratio impacts not just the amplitudes of the modes, but also the locations of the peaks in the CMB spectrum. In scenarios where neutrinos scatter off new light states during the period immediately prior to the CMB epoch, as in models of late time neutrino masses [46–48], and in the neutrinoless universe scenario [49], this ratio differs significantly from the SM prediction. Consequently, it has been possible to establish that this class of theories, which was already disfavored by the WMAP data [50–54], is now excluded by Planck, unless the new neutrino interactions come into equilibrium only very shortly prior to matter-radiation equality [55,56].

Similar considerations apply to the class of theories we are considering. In the presence of a new dark component of radiation, the free streaming fraction is altered, with the sign of the correction dependent on whether the DR scatters or free streams. Consequently, the amplitudes of the scalar and tensor modes receive corrections, with the sign of the effect dependent on whether the DR is free or self-interacting. In addition, the locations of the CMB peaks are shifted, with the sign of the shift again dependent on

[1]If the DM and DR are tightly coupled, oscillations of the DM-DR fluid can also give rise to signals in the matter power spectrum [32,33], (see also [34,35]). However, the large strength of the interaction required to obtain an observable effect would overly deplete the abundance of DM, and is therefore disfavored in the framework of thermal WIMPs.

whether or not the DR carries self-interactions. We find that these effects may be large enough to allow upcoming experiments to distinguish between free DR and scattering DR. Therefore the CMB offers a window into the dynamics of the hidden sector that DM annihilates into.

The outline of this paper is as follows. In the next section we discuss the CMB signals associated with DR, and explain how scenarios with free streaming DR and scattering DR can be distinguished. In Sec. III we show how the expression for the relic abundance of DM may be generalized to the case when the temperature of the dark sector differs from that of the SMIn Sec. IV we consider a simple model based on the Higgs portal that realizes this scenario, and show that the signals can be large enough to be detected by upcoming CMB experiments, while remaining compatible with the recent Planck results [1]. We also show that invisible decays of the Higgs into hidden sector states at colliders can offer a complementary probe of this scenario. Our conclusions are in Sec. V.

II. THE CMB SIGNALS OF DARK RADIATION

The CMB spectrum is affected by the presence of extra relativistic degrees of freedom during the era between matter-radiation equality and photon decoupling. It is customary in cosmology to quantify the contribution to the energy density from such additional radiation in units of the energy density of a single relativistic SM neutrino species $\rho_{1\nu}$,

$$\Delta N_{\rm eff} \equiv \frac{\rho_{\rm DR}}{\rho_{1\nu}}, \tag{1}$$

where $\rho_{\rm DR}$ is the energy density of DR, and all SM neutrinos are treated as being relativistic at the temperatures in question.

For any specific hidden sector model, we can calculate $\rho_{\rm DR}$, and hence $\Delta N_{\rm eff}$. The first step is to determine the temperature of the dark sector, $\hat{T}$, that corresponds to a given SM temperature T at the same cosmic time t. To do this, note that the comoving entropies of the SM and of the dark sector are separately conserved after the two sectors thermally decouple from each other. Then, after thermal decoupling when $T = \hat{T} = T_{\rm kd}$, but before the neutrino decoupling, taking the ratio of the two entropy conservation relations leads to the relation

$$\frac{\hat{g}_* \hat{T}^3}{g_* T^3} = \frac{\hat{g}_{*\rm kd}}{g_{*\rm kd}}. \tag{2}$$

Here g_* and $g_{*\rm kd}$ are the number of degrees of freedom in the SM at temperatures T and $T_{\rm kd}$, respectively, with the usual $7/8$ factors for the fermions. The corresponding parameters in the dark sector are labeled by $\hat{g}_*$ and $\hat{g}_{*\rm kd}$. Applying this relation just above the neutrino decoupling temperature $T \sim \mathcal{O}(10)$ MeV, $g_* = 10.75$, and noting that the contribution of a single neutrino species to the energy density is given by $\rho_{1\nu} = \frac{7}{4}\frac{\pi^2}{30} T^4$, we have

$$\Delta N_{\rm eff} = \frac{\hat{g}_* \hat{T}^4}{\frac{7}{4} T^4} = \frac{4}{7} \hat{g}_* \left(\frac{g_*}{\hat{g}_*} \frac{\hat{g}_{*\rm kd}}{g_{*\rm kd}} \right)^{4/3}. \tag{3}$$

Note that the above $\Delta N_{\rm eff}$ computed for the time just before neutrino decoupling is the same as the $\Delta N_{\rm eff}$ at the later CMB time, as $\hat{T}$ and T_ν redshifts the same way till then.

As outlined in section I, in general $\rho_{\rm DR}$ can consist of two qualitatively very different types of radiation: free-streaming radiation with mean free path $\gg H^{-1}$, and scattering radiation with mean free path $\ll H^{-1}$. We can parametrize each of these components of radiation in complete analogy with the definition (1),

$$\Delta N_{\rm eff}^{\rm free} \equiv \frac{\rho_{\rm DR}^{\rm free}}{\rho_{1\nu}}, \qquad \Delta N_{\rm eff}^{\rm scatt} \equiv \frac{\rho_{\rm DR}^{\rm scatt}}{\rho_{1\nu}}, \tag{4}$$

so that the total extra radiation $\Delta N_{\rm eff} = \Delta N_{\rm eff}^{\rm free} + \Delta N_{\rm eff}^{\rm scatt}$.

In this class of models, for a given thermal decoupling temperature $T_{\rm kd}$, there is a robust lower bound on $\Delta N_{\rm eff}$. To understand this, note that the lowest possible value of $\hat{g}_*$ in Eq. (3) is 1, corresponding to the case when the dark radiation consists of just a single real scalar. Then, if thermal decoupling between the hidden sector and the SM occurs at temperatures well below the mass of the DM particle, we can have $\hat{g}_{*\rm kd} = \hat{g}_* = 1$. In this limit we obtain a lower bound on $\Delta N_{\rm eff}$,

$$\Delta N_{\rm eff}^{\rm min} = \frac{4}{7} \left(\frac{g_*}{g_{*\rm kd}} \right)^{4/3}. \tag{5}$$

From Equation (5), assuming all the SM degrees of freedom are in the bath at decoupling, we have $g_{*\rm kd} = 106.75$, which leads to a lower bound on the effective number of neutrinos, $\Delta N_{\rm eff}^{\rm min} \gtrsim 0.027$. This result applies to arbitrarily high $T_{\rm kd}$ provided there are no new states in the SM sector up to that scale. In Fig. 1 we have plotted this lower bound as a function of the decoupling temperature $T_{\rm kd}$. Quite intriguingly, the ultimate experimental sensitivity at CMB-Stage-IV is $\sigma_{N_{\rm eff}} = 0.02$ [40], which would allow it to probe the DM scenario we outline here. This projected experimental sensitivity is based on a one parameter extension of the standard six parameter ΛCDM model that accommodates varying $N_{\rm eff}$. Although this projection assumes that the primordial density fluctuations have an exactly power law spectrum, the recent Planck results have established that at present this is an excellent fit to data [1], and so this forms a reasonable basis for estimating the sensitivity.

If the dark sector consists of just a real scalar, we expect that it is a Goldstone boson, so that its mass is protected against radiative corrections from the weak scale. In this

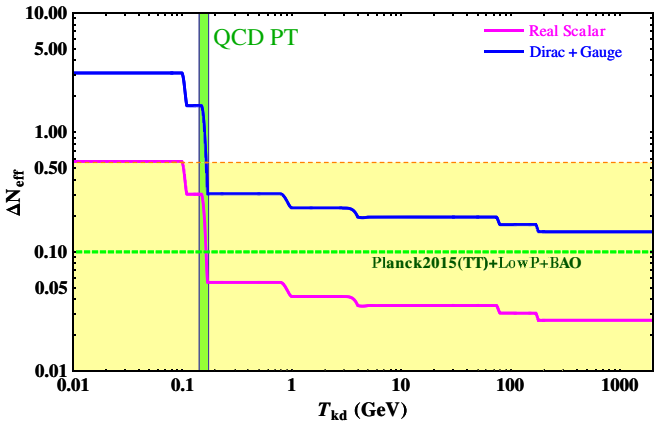

FIG. 1 (color online). $\Delta N_{\rm eff}$ as a function of the temperature at which the SM and dark sector thermally decouple. Also shown are the 2015 Planck results: the central value (green dashed line) and the 2σ constraint (orange dashed line).

scenario, the interactions of the states that constitute the DR are momentum suppressed, and so the DR free streams. In scenarios where the DR possesses self-interactions large enough to prevent free streaming, the requirement of naturalness up to the weak scale implies that it must be composed of more than just a single real scalar, or else the radiative corrections to the scalar mass from the self-interactions would tend to make its mass much greater than an eV. Therefore, in scenarios where the DR scatters, we expect that there will be additional light states in the hidden sector, and so $\Delta N_{\rm eff}$ is expected to be larger than its minimum value, $\Delta N_{\rm eff}^{\rm min}$. In Fig. 1, we have plotted $\Delta N_{\rm eff}$ as a function of $T_{\rm kd}$ for the case when the DR consists of a pair of massless Weyl fermions with vectorlike charges under a U(1) gauge group, and the associated massless gauge boson. We see that even for high $T_{\rm kd}$, we predict $\Delta N_{\rm eff} \gtrsim 0.15$, which is large enough to be observed at CMBPol.

In the rest of this section we discuss how the experimental limits on $\Delta N_{\rm eff}$ are obtained, and how we can distinguish between the two cases of scattering DR and free streaming DR.

A. The determination of $\Delta N_{\rm eff}$

At present, limits on $\Delta N_{\rm eff}$ are obtained by considering how the presence of additional energy density in radiation would affect the quality of the fit in the six parameter ΛCDM model. Of the six parameters, two are particularly sensitive to $\Delta N_{\rm eff}$. These are the total energy density in matter, ρ_m, which is the sum of the energy densities in baryons and DM, and in the cosmological constant, ρ_Λ. The presence of additional energy density in radiation would tend to delay the onset of matter-radiation equality. Since the amplitude of a Fourier mode is very sensitive to the fraction of energy density in matter as it crosses the horizon, this ratio is highly constrained by the CMB data. Therefore, for $\Delta N_{\rm eff} > 0$, the best fit is obtained by increasing ρ_m in the appropriate proportion to ensure that the redshift at the onset of matter-radiation equality is unaffected. Since the energy density in baryons, ρ_b, is very tightly constrained by measurements of the relative heights of the even and odd CMB peaks and cannot be altered, the change in ρ_m is accomplished by an increase in the energy density in DM.

The additional energy density in DR, and in matter, then implies an increase in the Hubble constant during the CMB epoch. This will in turn affect the size of the sound horizon, leading to a change in the locations of the CMB peaks. This observable is, once again, highly constrained by the data. However, this effect can be offset by changing ρ_Λ so as to alter the distance to the last scattering surface, thereby keeping the angular locations of the peaks intact. Nevertheless, as we now explain, the change in the Hubble constant during the era of acoustic oscillations leads to other effects in the CMB spectrum that can no longer be compensated for once ρ_m and ρ_Λ are fixed.

Prior to recombination, the photons interacted strongly with the baryons. Although the photon mean free path during this era was relatively short, the photons were nevertheless able to diffuse outward, with a characteristic diffusion length r_d. As a consequence of this diffusion, inhomogeneities and anisotropies at scale smaller than the r_d are suppressed. This damps the peak amplitudes at higher ℓ relative to the first peak at $\ell \simeq 220$, which corresponds to modes that entered the horizon near recombination. This effect is known as Silk damping, or diffusion damping. A change in the Hubble rate affects the time available for diffusion, leading to observable effects on the CMB spectrum. In particular, the height of the first CMB acoustic peak relative to the latter peaks is altered. Therefore, this effect can be used to place limits on the Hubble constant during the epoch of acoustic oscillations, and therefore on $\Delta N_{\rm eff}$. The presence of additional energy density in radiation also leads to changes in the CMB spectrum associated with the early integrated Sachs-Wolfe (ISW) effect, but these are less significant than the effects arising from Silk damping [57].

In principle, an increase in the fraction of baryons in helium, $Y_{\rm He}$, while ρ_b is held fixed, would reduce the number of free electrons available for scattering, and could also account for a change in the scale of Silk damping. However, the helium fraction in the SM can be calculated sufficiently precisely from big bang nucleosynthesis so as to exclude this as the explanation for any observed discrepancy. For a good discussion of these issues with more details, see [57,58].

B. Distinguishing between free and scattering DR via scalar metric perturbations

Several authors have considered the effects of the SM neutrinos on the scalar component of the CMB

spectrum [41–43]. These results can easily be generalized to the case when there is additional energy density in radiation, and can be used to distinguish between free streaming DR and scattering DR.

In the conformal Newtonian gauge the Robertson-Walker metric with scalar perturbations takes the form,

$$ds^2 = a^2(\tau)(-(1+2\Phi)d\tau^2 + (1-2\Psi)d\mathbf{r}^2). \quad (6)$$

Here τ represents conformal time, while a is the cosmological scale factor. Ψ and Φ represent the scalar metric perturbations. In the absence of any free streaming particle species, we have $\Psi = \Phi$. When, however, a free streaming species is present, the energy momentum tensor becomes anisotropic. This leads to a difference between Ψ and Φ that is proportional to f_ν, the total energy density in free streaming radiation expressed as a fraction of the total energy density in radiation.

$$f_\nu \equiv \frac{\rho_{\text{all free rad}}}{\rho_{\text{all rad}}} = \frac{3\rho_{1\nu} + \rho_{\text{DR}}^{\text{free}}}{3\rho_{1\nu} + \rho_\gamma + \rho_{\text{DR}}^{\text{free}} + \rho_{\text{DR}}^{\text{scatt}}}. \quad (7)$$

In the limit that $\rho_{\text{DR}}^{\text{free}}$ and $\rho_{\text{DR}}^{\text{scatt}}$ are small compared to $\rho_{\text{all rad}}$, the total energy density in radiation, the deviation from the standard cosmology is given by

$$\begin{aligned} f_\nu - f_\nu|_{\text{SM}} &= \frac{f_\nu|_{\text{SM}}}{3}[(1 - f_\nu|_{\text{SM}})\Delta N_{\text{eff}}^{\text{free}} - f_\nu|_{\text{SM}}\Delta N_{\text{eff}}^{\text{scatt}}] \\ &= \frac{0.41}{3}(0.59\Delta N_{\text{eff}}^{\text{free}} - 0.41\Delta N_{\text{eff}}^{\text{scatt}}). \end{aligned} \quad (8)$$

Now, the solution of the coupled system of equations for matter, radiation and gravity reveals that the presence of a free streaming component in radiation is associated with a change in the amplitudes of the CMB modes at large ℓ. The magnitude of this effect was first determined numerically in [41]. Subsequently, analytic expressions were obtained in [42,43]. The result is given by,

$$\frac{\delta C_\ell}{C_\ell} = -\frac{8}{15} f_\nu. \quad (9)$$

Then, using Eq. (8), we can obtain an expression for the fractional change in C_ℓ with respect to the standard cosmology,

$$\begin{aligned} \frac{\Delta C_\ell}{C_\ell} &= \frac{\delta C_\ell}{C_\ell} - \left.\frac{\delta C_\ell}{C_\ell}\right|_{\text{SM}} \\ &= -\frac{8}{15}(f_\nu - f_\nu|_{\text{SM}}) \\ &= -0.072(0.59\Delta N_{\text{eff}}^{\text{free}} - 0.41\Delta N_{\text{eff}}^{\text{scatt}}). \end{aligned} \quad (10)$$

We see that the result is independent of ℓ, and that the sign of this effect depends on whether the DR is scattering or free streaming.

In addition to the corrections to the amplitude, there is a shift in the angular locations of the high ℓ CMB peaks by an equal amount [43]. This signal is particularly important because, in contrast to other effects of DR such as Silk damping, it is difficult to mimic by altering other parameters such as the helium fraction. The magnitude of this shift is again proportional to the free streaming fraction f_ν,

$$\delta\ell \simeq -57 f_\nu \frac{\ell_{\text{A}}}{300}. \quad (11)$$

Here $\ell_{\text{A}} \approx 300$ represents the average angular spacing between the CMB peaks at large ℓ. Again, in the limit that DR contributes only a small fraction of the total energy in radiation, $\Delta N_{\text{eff}} \lesssim 1$, Eq. (8) leads to an expression for the change in $\delta\ell$ with respect to the standard cosmology,

$$\begin{aligned} \Delta\ell &\equiv \delta\ell - \delta\ell|_{\text{SM}} \\ &= -57(f_\nu - f_\nu|_{\text{SM}})\frac{\ell_{\text{A}}}{300} \\ &\simeq -7.8(0.59\Delta N_{\text{eff}}^{\text{free}} - 0.41\Delta N_{\text{eff}}^{\text{scatt}})\frac{\ell_{\text{A}}}{300}. \end{aligned} \quad (12)$$

Once again we see that the sign of the effect depends on whether the DR is scattering or free streaming.

We can obtain a very rough estimate of the sensitivity of upcoming CMB experiments to the effects of $\Delta\ell$ by considering how well N_{eff} can be determined when the helium fraction Y_{He} is allowed to float freely. In this limit, the effects of ΔN_{eff} on Silk damping can be compensated for by changes in Y_{He}. Under these circumstances, the shifts in the locations of the CMB peaks play an important role in the determination of N_{eff}, and we can interpret the results as a rough guide to the sensitivity of these experiments to ΔN_{eff} arising from its effect on $\Delta\ell$, and not its effect on Silk damping. The projected sensitivity of CMBPol to N_{eff} when Y_{He} is allowed to float is $\Delta N_{\text{eff}} = 0.09$ [43]. We therefore expect that provided $\Delta N_{\text{eff}} \gtrsim 0.10$, upcoming experiments will have some sensitivity to whether DR is free streaming or scattering, allowing the possibility of distinguishing between these two scenarios.

C. Distinguishing between free and scattering DR via tensor metric perturbations

The presence of a free streaming component of radiation also affects the tensor component of the CMB spectrum. Detailed studies of the effects of the SM neutrinos on the tensor modes (the B- and E-modes) of the CMB were performed in [44,45], which found an $\mathcal{O}(10)\%$ damping of the correlation functions of the tensor modes at long wavelengths, rising to an $\mathcal{O}(35)\%$ damping at short wavelengths. Analytic results for the damping were subsequently obtained in [59,60]. The corrections to the spectrum that arise from the presence of a free streaming DR component were considered in [61].

We now show that the results of [44] can be generalized in a very simple way to arbitrary $N_{\rm eff}$, provided $\Delta N_{\rm eff} \lesssim 1$. The crucial observation is that, in the analysis of [44], the effects of the SM neutrinos arise entirely from their contribution to $\bar{f}_\nu$, the free-streaming fraction of the total energy density,

$$\bar{f}_\nu \equiv \frac{\rho_{\text{all free rad}}}{\rho_{\rm total}} = \frac{3\rho_{1\nu} + \rho_{\rm DR}^{\rm free}}{\rho_{\rm total}}. \tag{13}$$

Therefore, by understanding how the result depends on $\bar{f}_\nu$, we can immediately determine how the correlation functions of the tensor modes depend on $\Delta N_{\rm eff}^{\rm free}$ and $\Delta N_{\rm eff}^{\rm scatt}$. During the radiation dominated era, to a very good approximation, $\bar{f}_\nu = f_\nu$. However, as matter-radiation equality approaches, the contribution of matter to the total energy density can no longer be neglected, and $\bar{f}_\nu$ and f_ν are distinct.

The Robertson-Walker metric with tensor perturbations takes the form,

$$ds^2 = a^2(\tau)(-d\tau^2 + [\delta_{ij} + h_{ij}(\mathbf{x},\tau)]dx^i dx^j) \tag{14}$$

with $h_{ii} = \partial_i h_{ij} = 0$. We define a new coordinate $u = k\tau$, where k is the comoving wave number. Then, as shown in [44], the amplitude of tensor perturbations with comoving wave number k can be written as $h_{ij}(u) = h_{ij}(0)\chi(u)$, where the function $\chi(u)$ remains to be determined. It satisfies the integro-differential equation

$$\mathcal{F}(u,\partial_u)\chi(u) = \bar{f}_\nu \int_0^u \mathcal{I}(u,U)\chi'(U)dU, \tag{15}$$

where $\mathcal{F}(u,\partial_u)$ is a second-order, linear differential operator. Its precise form, along with that of the kernel function $\mathcal{I}(u,U)$, may be found in [44]. The initial conditions on χ are given by $\chi(0) = 1$ and $\chi'(0) = 0$.

In general, the integro-differential equation Eq. (15) is not simple to solve. However, approximate analytic solutions that apply in certain limits have been obtained for the important case of the SM with 3 free streaming neutrinos, $N_{\rm eff} = 3.046$. As we now explain, these solutions can be generalized in a simple way to the case of arbitrary $\bar{f}_\nu$, provided $\Delta N_{\rm eff} \lesssim 1$.

For *short wavelengths* that enter the horizon well before matter radiation equality, that is, $u \gg 1$, the solution to Eq. (15) approaches a homogeneous solution [44],

$$\chi(u) \to A\frac{\sin(u+\delta)}{u}, \tag{16}$$

where the parameters A and δ contain the dependence on $\bar{f}_\nu = f_\nu$. In the limit $f_\nu = 0$, A and δ take values $A_0 = 1, \delta_0 = 0$. We denote this solution by $\chi_0(u)$. For the case of the three free streaming neutrino species of the SM, with $f_\nu = f_\nu^{\rm SM} = 0.41$, a numerical study [44] leads to the values $A_{\rm SM} = 0.80, \delta_{\rm SM} \approx 0$. The fact that the value of A changes by only about 20% for the change from $N_{\rm eff} = 0$ to $N_{\rm eff} = 3.046$ indicates that for $\Delta N_{\rm eff} \lesssim 1$ the term proportional to f_ν can be treated as a perturbation. Accordingly, we may obtain an approximate solution for general f_ν by replacing $\chi(u)$ by $\chi_{\rm SM}(u)$ on the right-hand side of Eq. (15). Here $\chi_{\rm SM}(u)$ is the solution of Eq. (15) for $f_\nu = f_\nu^{\rm SM}$. Having made this approximation, Eq. (15) reduces to

$$\mathcal{F}(u,\partial_u)\chi(u) = f_\nu \int_0^u \mathcal{I}(u,U)\chi'_{\rm SM}(U)dU. \tag{17}$$

Noting that the right-hand side of this equation is proportional to $\mathcal{F}(u,\partial_u)\chi_{\rm SM}(u)$, we have

$$\mathcal{F}(u,\partial_u)\left(\chi(u) - \frac{f_\nu}{f_\nu^{\rm SM}}\chi_{\rm SM}(u)\right) = 0. \tag{18}$$

Recalling that $\mathcal{F}(u,\partial_u)\chi_0(u) = 0$, it follows that this equation admits a solution of the form,

$$\chi(u) - \frac{f_\nu}{f_\nu^{\rm SM}}\chi_{\rm SM}(u) \propto \chi_0(u). \tag{19}$$

Using the initial conditions to fix the constant of proportionality, we obtain an analytic solution for $\chi(u)$ valid for general f_ν that is applicable in the short-wavelength limit,

$$\chi(u) = \left(1 + \frac{f_\nu}{f_\nu^{\rm SM}}(A_{\rm SM} - 1)\right)\frac{\sin u}{u}. \tag{20}$$

As discussed in [44], the ratio of the CMB tensor correlation functions for general f_ν *relative to* that for $f_\nu^{\rm SM}$ is given by

$$R = \left|\frac{\chi'(u)}{\chi'_{\rm SM}(u)}\right|^2 = \frac{(1 + \frac{f_\nu}{f_\nu^{\rm SM}}(A_{\rm SM} - 1))^2}{A_{\rm SM}^2}. \tag{21}$$

Since the right-hand side of this equation is independent of u, it follows that the fractional change in the correlation functions arising from the presence of DR is independent of wave number for modes deep inside the horizon. The result is plotted in Fig. 2.

To obtain the solution of Eq. (15) for *long wavelengths*, it is convenient to change variables from u to $y \equiv a(\tau)/a(\tau_{\rm eq})$, where $a(\tau)$ is the standard scale factor of the Robertson-Walker metric and $\tau_{\rm eq}$ is the value of the conformal time coordinate τ at matter-radiation equality. Expressed in terms of y, the integro-differential equation Eq. (15) takes the form

$$[\mathcal{G}(y,\partial_y) + Q^2]\chi(y) = f_\nu \int_0^y \mathcal{J}(y,Y)\chi'(Y)dY. \tag{22}$$

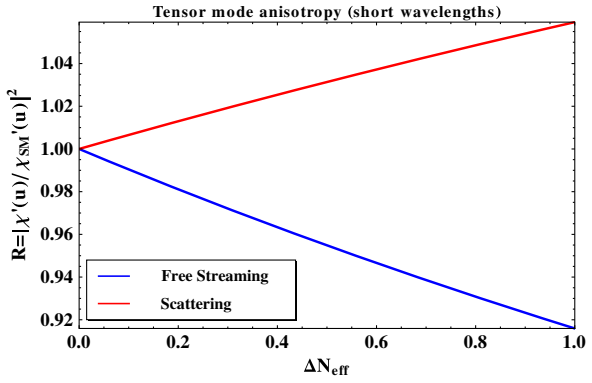

FIG. 2 (color online). Relative change in tensor mode anisotropy compared to the SM case ($N_{\rm eff} = 3.046$), $R = \left|\frac{\chi'(u)}{\chi'_{\rm SM}(u)}\right|^2$, for short wavelengths.

Here $\mathcal{G}(y, \partial_y)$ is again a second-order, linear differential operator, and Q is a normalized comoving wave number defined as $Q \equiv \sqrt{2}k/k_{\rm eq}$, where $k_{\rm eq}$ is the value of k corresponding to the length scale that enters the horizon at matter-radiation equality. We have also eliminated $\bar{f}_\nu(y)$ in favor of f_ν, which is independent of y. The initial conditions are now given by $\chi(0) = 1$ and $\chi'(0) = 0$. The precise forms of $\mathcal{G}$ and the kernel function $\mathcal{J}(y, Y)$ may be found in [44]. Then, given the solutions $\chi_0(y)$ and $\chi_{\rm SM}(y)$ corresponding to the choices $f_\nu = 0$ and $f_\nu = f_\nu^{\rm SM}(y)$, an approximate solution $\chi(y)$ corresponding to a general f_ν may be obtained as

$$\chi(y) = \chi_0(y) + \frac{f_\nu}{f_\nu^{\rm SM}}(\chi_{\rm SM}(y) - \chi_0(y)). \tag{23}$$

Expressions for $\chi'_{\rm SM}(y_{\rm dec})$ and $\chi'_0(y_{\rm dec})$ at small Q were obtained in [60],

$$\begin{aligned}\chi'_{\rm SM}(y_{\rm dec}) &= a_2 Q^2 + a_4 Q^4 + a_6 Q^6 + \mathcal{O}(Q^8),\\ \chi'_0(y_{\rm dec}) &= b_2 Q^2 + b_4 Q^4 + b_6 Q^6 + \mathcal{O}(Q^8),\end{aligned} \tag{24}$$

with

$$\begin{aligned} a_2 &= -0.573661, \quad a_4 = 0.243294, \quad a_6 = -0.0381643,\\ b_2 &= -0.601254, \quad b_4 = 0.264482, \quad b_6 = -0.0424186.\end{aligned}$$

Here $y_{\rm dec}$ is the value of y at photon decoupling, given by $y_{\rm dec} = 3.31$. Note that the regime of validity of these expansions is limited to small Q, and they are expected to break down at $Q \sim 1$. Nonetheless these analytic approximations offer a simple way to parametrize the effects of DR on the tensor mode anisotropies for long wavelengths. Using these expressions in association with the general solution Eq. (23), we can determine the suppression of the tensor correlation function for arbitrary f_ν relative to that for the SM,

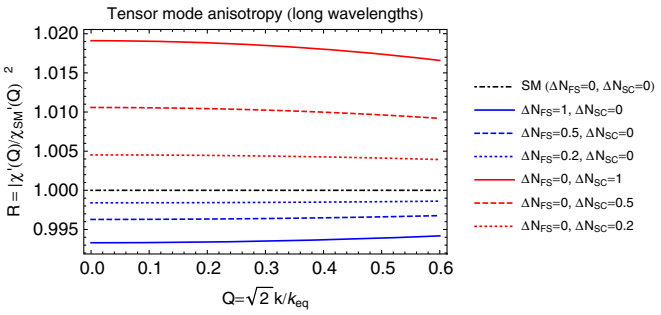

FIG. 3 (color online). Relative change in tensor mode anisotropy compared to the SM case ($N_{\rm eff} = 3.046$), $R = \left|\frac{\chi'(y_{\rm dec})}{\chi'_{\rm SM}(y_{\rm dec})}\right|^2$, for varying $\Delta N_{\rm eff}^{\rm free}$ (shorthand $\Delta N_{\rm FS}$) and $\Delta N_{\rm eff}^{\rm scatt}$ (shorthand $\Delta N_{\rm SC}$), for long wavelengths.

$$R = \left|\frac{\chi'(y_{\rm dec})}{\chi'_{\rm SM}(y_{\rm dec})}\right|^2. \tag{25}$$

The results are shown in Fig. 3, where we can see that scattering and free streaming DR contribute with opposite signs. It follows that while scattering DR tends to reduce the damping effect associated with the SM neutrinos, free streaming DR enhances this effect. This dissimilar behavior is analogous to what was observed for the corrections to the amplitude and phase of the scalar modes.

III. DETERMINATION OF THE RELIC ABUNDANCE

In this section we explain how the well-known formalism for determining the relic abundance of DM generalizes to the case when the DM sector and the SM are at two different temperatures. The evolution of the DM density in an expanding universe is governed by the Boltzmann equation,

$$\frac{{\rm d}n_\chi}{{\rm d}t} + 3Hn_\chi = -\langle\sigma v\rangle(n_\chi^2 - (n_\chi^{\rm eq})^2). \tag{26}$$

The difference between the scenario we are considering and the conventional relic abundance calculation for a thermal WIMP lies in the fact that in Eq. (26), the averaged annihilation cross section $\langle\sigma v\rangle$ and the DM equilibrium number density $n_\chi^{\rm eq}$ now depend on the dark sector temperature $\hat{T}$ rather than the SM temperature T, while the Hubble constant H depends on both T and $\hat{T}$. In our analysis we will assume that at temperatures in the neighborhood of the freeze-out, the number of relativistic degrees of freedom in the SM, and in the dark sector, are not changing. Then, since the entropy densities of the two sectors are separately conserved, it follows that during freeze-out the ratio of the dark sector temperature $\hat{T}$ to the SM temperature T is a constant labeled by $r \equiv \hat{T}/T$. We can then express all the terms in the Boltzmann equation as functions of the SM

temperature T. For the equilibrium number density in the nonrelativistic limit we have,

$$n_\chi^{\rm eq}(\hat{T}) = g_\chi \left(\frac{m_\chi \hat{T}}{2\pi}\right)^{\frac{3}{2}} e^{-\frac{m_\chi}{\hat{T}}} = g_\chi \left(\frac{r m_\chi T}{2\pi}\right)^{\frac{3}{2}} e^{-\frac{m_\chi}{rT}}. \quad (27)$$

For the Hubble constant,

$$H^2 = \frac{8\pi G}{3}\rho = \frac{8\pi}{3M_{\rm P}^2}(\rho_{\rm SM} + \rho_{\rm dark}) = \frac{8\pi}{3M_{\rm P}^2}\left(\frac{\pi^2}{30} g_*(T) T^4 + \frac{\pi^2}{30}\hat{g}_*(\hat{T})\hat{T}^4\right) \equiv \frac{4\pi^3}{45 M_{\rm P}^2} g_{*\rm eff} T^4, \quad (28)$$

where

$$g_{*\rm eff}(T,\hat{T}) \equiv g_*(T) + \hat{g}_*(\hat{T})\left(\frac{\hat{T}}{T}\right)^4 = g_*(T) + \hat{g}_*(\hat{T}) r^4. \quad (29)$$

In the nonrelativistic regime $\langle\sigma v\rangle$ is well approximated by

$$\langle\sigma v\rangle = a + b\langle v^2\rangle \quad (30)$$

where the constant term plays the leading role if the annihilation can proceed through the s-wave. If, however, the s-wave contribution is suppressed so that annihilation occurs primarily through the p-wave, the term proportional to v^2 dominates. Performing the thermal average,

$$a + b\langle v^2\rangle = a + 6rb\frac{T}{m_\chi}. \quad (31)$$

We are now in a position to solve the Boltzmann equation by the standard procedure. We introduce the variable $Y \equiv n_\chi/s_{\rm SM}$, where $s_{\rm SM}$ is the entropy density carried by the SM degrees of freedom. We also introduce the variable $x \equiv m_\chi/T$. In the radiation dominated era, when g_* and $\hat{g}_*$ are not changing, we have

$$\frac{dx}{dt} = Hx. \quad (32)$$

Eliminating the number density n_χ in favor of Y, and t in favor of x, we obtain for the Boltzmann equation,

$$\frac{dY}{dx} = -\frac{\langle\sigma v\rangle}{Hx} s_{\rm SM}(Y^2 - Y_{\rm eq}^2). \quad (33)$$

Rewriting this in terms of $\Delta \equiv Y - Y_{\rm eq}$, we have

$$\Delta' = -Y'_{\rm eq} - f(x)\Delta(2Y_{\rm eq} + \Delta), \quad (34)$$

where $f(x)$ is given by

$$f(x) \equiv \frac{\langle\sigma v\rangle s_{\rm SM}}{Hx} = \sqrt{\frac{\pi}{45}}\frac{g_*}{\sqrt{g_{*\rm eff}}} m_\chi M_{\rm P}\frac{a + 6rb/x}{x^2}. \quad (35)$$

This Boltzmann equation cannot be solved exactly. However, it is possible to obtain analytic solutions of this equation that are valid at very early times, and very late times. Then, an approximate solution that is valid for all times may be obtained by stitching together these limiting cases. We define the freeze-out temperature T_f in terms of the implicit relation,

$$\Delta(x_f) = cY_{\rm eq}(x_f), \quad (36)$$

where c is an order one number. The final result depends only logarithmically on the value of c, which is chosen to be $\sqrt{2}-1$ in the case of s-wave annihilation and $\sqrt{3}-1$ in the case of p-wave annihilation, to give the best fit to numerical results [62]. At early times $x \ll x_f$, $\Delta' \ll Y'_{\rm eq}$, so that the Boltzmann equation reduces to

$$\Delta = -\frac{Y'_{\rm eq}}{f(x)(2Y_{\rm eq} + \Delta)}. \quad (37)$$

This equation, in combination with Eq. (36), may be used to determine the freeze-out temperature,

$$x_f = r\log\left(\frac{c(c+2)}{4\pi^3}\sqrt{\frac{45}{2}}\frac{g_\chi}{\sqrt{g_{*\rm eff}}} m_\chi M_{\rm P}\frac{r^{\frac{5}{2}}(a + 6rb/x_f)}{x_f^{1/2}}\right). \quad (38)$$

At late times, $x \gg x_f$, $\Delta \approx Y \gg Y_{\rm eq}$ and $\Delta' \gg Y'_{\rm eq}$ so that we have,

$$Y^{-2}Y' = -f(x). \quad (39)$$

Integrating this equation from x_f to ∞, we obtain

$$Y_\infty = \left[\sqrt{\frac{\pi}{45}}\frac{g_*}{\sqrt{g_{*\rm eff}}} M_{\rm P} m_\chi \frac{a + 3rb/x_f}{x_f}\right]^{-1} \quad (40)$$

where we have used the fact that $\Delta(x_f) \gg \Delta(\infty)$. Combining this result with the expression for x_f from Eq. (38), we can obtain the present-day energy density in dark matter, $\Omega_\chi = m_\chi s_0 Y_\infty \rho_c^{-1}$. Here s_0, ρ_c are the present-day SM entropy density and critical density, respectively.

From this discussion we see that the difference between our framework, which allows for $\hat{T} \neq T$ at freeze-out, and the conventional scenario with $\hat{T} = T$, primarily translates into an extra factor of $r = \hat{T}/T$ in the expression for the

relic abundance of DM. There is an additional effect arising from the r dependence of the argument of the logarithm in Eq. (38), but this is small. Put in another way, the values of a and b in the expression for $\langle\sigma v\rangle$ in Eq. (30) that correspond to the observed $\Omega_{\rm DM}$ are smaller by a factor of $\hat{T}/T$ than in the case of the standard thermal cross section $\sim 3\times 10^{-26}$ cm^3/s. One may obtain similar results to those given in Eqs. (38) and (40) by performing a simple estimate based on equating $\Gamma_\chi = n_\chi^{\rm eq}\langle\sigma v\rangle$ to the Hubble constant H at freeze-out, while keeping track of the distinction between T and $\hat{T}$.

In this analysis, we have assumed that the number of degrees of freedom in the SM, and in the hidden sector, do not change in the neighborhood of the freeze-out temperature. We have further assumed that the annihilation cross section is well approximated by an expansion of the form given in Eq. (31). Using the methods of [63,64], these assumptions can be relaxed, and the result generalized. We leave this for future work.

IV. A SIMPLE BENCHMARK MODEL

A. The model

In this section we consider in detail a simple model that illustrates the scenario we are considering. We consider an unbroken U(1) gauge theory with massless spin-1/2 fermions charged under it. Let $\hat{A}_\mu$ be the massless gauge boson associated with this U(1), and $\hat{\psi}_i$ and $\hat{e}_i$ $(i = 1, 2, \ldots, N_{\hat{\psi}})$ represent the massless (4 component) fermions and their associated charges under $\mathrm{U}(1)_{\hat{A}}$. Note that some of the $\hat{e}_i$ may be zero, thereby allowing us to dial the number of free-streaming species. We consider a complex scalar particle, denoted by χ, as the DM candidate.

Since our scenario assumes hidden sector dark matter, χ is uncharged under the SM gauge interactions. The only possible renormalizable interaction of χ with SM particles is of the Higgs portal form $|\chi|^2|H|^2$, where H is the complex scalar doublet that includes the SM Higgs particle h. This operator is expected to be present, and serves to ensure that the SM and hidden sectors are initially in thermal and chemical equilibrium. However, our interest is in the scenario in which this coupling is not large enough to govern the annihilation of dark matter that determines its relic abundance. Instead, the relic abundance is controlled by an additional interaction through which dark matter annihilates into DR. For that purpose, we introduce a massive spin-1 boson $\hat{Z}$ that couples to both χ and $\hat{\psi}_i$, which carry charges $\hat{q}_\chi$ and $\hat{q}_i$ under the associated broken $\mathrm{U}(1)_{\hat{Z}}$. In our analysis, we will focus on the parameter range where χ is lighter than the $\hat{Z}$ gauge boson by a factor of a few.

The Lagrangian of our benchmark model therefore reads as

$$\begin{aligned}\mathcal{L} = \mathcal{L}_{\rm SM} + (\mathrm{D}_\mu\chi)^*(\mathrm{D}^\mu\chi) - \hat{m}_\chi^2|\chi|^2 - \kappa|\chi|^2|H|^2 - \frac{\lambda}{4}|\chi|^4 \\ + \bar{\hat{\psi}}^i i\not{\mathrm{D}}\hat{\psi}_i - \frac{1}{4}\hat{Z}_{\mu\nu}\hat{Z}^{\mu\nu} + \frac{1}{2}m_{\hat{Z}}^2\hat{Z}^2 - \frac{1}{4}\hat{A}_{\mu\nu}\hat{A}^{\mu\nu} \\ + \cdots \end{aligned} \tag{41}$$

In this expression the ellipses represents the sector responsible for breaking $\mathrm{U}(1)_{\hat{Z}}$ and generating the $\hat{Z}$ mass. We will not specify this sector explicitly as it is not relevant for our discussions. We only mention that all the particles in that sector are assumed to be significantly heavier than m_χ and $m_{\hat{Z}}$, so that they do not affect the dynamics we are considering.[2] Note that, as a consequence of electroweak symmetry breaking, the parameter $\hat{m}_\chi$ in the Lagrangian is not equal to the χ mass, m_χ, but is related to it as

$$m_\chi^2 = \hat{m}_\chi^2 + \frac{\kappa}{2}v_{\rm EW}^2, \tag{42}$$

where $v_{\rm EW} = 246$ GeV. The masses of the $\hat{\psi}_i$ are all set to zero, and are protected against quantum corrections by chiral symmetry. Finally, to ensure the stability of the dark matter particle χ, we impose an exact $\mathbb{Z}_2$ symmetry under which χ is odd and all the other fields are even.[3]

In this benchmark model, there is only one renormalizable interaction, $\kappa|\chi|^2|H|^2$, that connects the dark sector to the SM. The presence of such an interaction is expected to be a general feature of any theory in which the dark matter particle is a scalar, as there is no symmetry that forbids it. Provided $\kappa \gtrsim 10^{-6}$, this coupling ensures that the SM and hidden sector are initially in thermal equilibrium at temperatures of order the weak scale. The requirement that annihilation to SM states does not play a significant role in setting the relic abundance constrains $\kappa \lesssim 10^{-2}$. We will therefore focus on the regime $10^{-2} \gtrsim \kappa \gtrsim 10^{-6}$. We also choose to stay away from the region of parameter space such that the DM mass is close to half the Higgs mass, where annihilation to the SM is resonantly enhanced.

The presence of interactions between the hidden sector and the SM leads to constraints on the theory and potential signals. Upon electroweak symmetry breaking, the $|\chi|^2|H|^2$ term leads to a 3-point interaction of the form $h|\chi|^2$. Provided $m_\chi < m_h/2$, this will generate a contribution to the invisible width of the Higgs boson given by

[2]We assume that the Lagrangian in Eq. (41) does not include kinetic mixings between these new U(1) gauge fields and those of the SM, such as $\hat{A}_{\mu\nu}B^{\mu\nu}$, where B_μ is the SM hypercharge gauge boson. These can be forbidden by an internal charge conjugation symmetry carried by the hidden sector fields.

[3]Alternatively, such $\mathbb{Z}_2$ symmetry can accidentally emerge if the value of $\hat{q}_\chi$ is such that it is not equal to any linear combination of the other $\mathrm{U}(1)_{\hat{Z}}$ charges with rational coefficients.

$$\Gamma_h^{\rm inv} = \frac{m_h}{16\pi}\frac{\kappa^2 v_{\rm EW}^2}{m_h^2}\beta_\chi, \qquad \beta_\chi \equiv \sqrt{1-\frac{4m_\chi^2}{m_h^2}}. \tag{43}$$

The current experimental limit on the invisible branching ratio from the LHC 7 and 8 TeV data sets stands at about 30% of the total Higgs width, $\Gamma_h = 4.07 \times 10^{-3}$ GeV, from the vector boson fusion channel [65,66]. The limit from the associated production channel is significantly weaker [67,68]. The bound on the invisible width is expected to improve to ~10% of the total width after 300 fb^{-1} at the 14 TeV LHC [69,70]. For $m_h \gg m_\chi$, these limits can be translated into the constraints on the parameter κ. At present we have $\kappa \lesssim 2 \times 10^{-2}$ from the LHC 7 and 8 TeV runs. This limit is expected to improve to $\kappa \lesssim 7 \times 10^{-3}$ after 300 fb^{-1} at the 14 TeV LHC. Stronger bounds can be obtained at future lepton colliders, such as the ILC or TLEP. According to the studies [71–73] these machines can constrain the Higgs invisible branching ratio to 0.2%–1%, which corresponds to $\kappa \lesssim 9.5 \times 10^{-4}$–$2.5 \times 10^{-3}$. For $m_h < 2m_\chi$, on-shell Higgs decays into DM particles are kinematically forbidden, and the hidden sector must be accessed through an off-shell Higgs, or through loop effects. The current collider limits are then very weak in the regime of interest, $\kappa \lesssim 10^{-2}$, and are not expected to improve significantly even at future colliders [72]. While the $h|\chi|^2$ interaction can also give rise to signals in direct/indirect DM detection experiments, current experiments are not yet sensitive in the region $\kappa \lesssim 10^{-2}$.

B. Relic abundance of DM

Let us now analyze this benchmark model. The first step is to require that the relic abundance of χ agree with the observed amount of cold dark matter. We focus on the region of parameter space where the DM mass lies between 5 GeV and 100 GeV, and where $2m_\chi < m_{\hat{Z}}$. Then the abundance of DM is governed by the annihilation process $\chi + \chi^* \to \hat{\psi} + \bar{\hat{\psi}}$ via the exchange of a virtual $\hat{Z}$ in the s-channel, after the DM particles become nonrelativistic. To lowest order in the nonrelativistic limit, the cross section for this process is given by

$$\sigma_{\chi\chi^*\to\hat{\psi}\bar{\hat{\psi}}} = \frac{\hat{g}_{\rm eff}^4}{48\pi m_\chi^2}\left(1-\frac{m_{\hat{Z}}^2}{4m_\chi^2}\right)^{-2} v_\chi, \tag{44}$$

where

$$\hat{g}_{\rm eff}^4 \equiv \sum_{i=1}^{N_{\hat{\psi}}} \hat{g}_Z^4 \hat{q}_\chi^2 \hat{q}_i^2 \tag{45}$$

and v_χ represents the speed of each annihilating χ in the center-of-momentum (CM) frame. The presence of the v_χ suppression is an indication that the annihilation process proceeds through the p-wave channel. This can be understood from the fact that the initial state consists of two scalars and the intermediate state is spin-1. Letting v be the relative velocity of the annihilating χ's ($v = 2v_\chi$), and performing a thermal averaging, we obtain

$$\langle \sigma_{\chi\chi^*\to\hat{\psi}\bar{\hat{\psi}}} v\rangle = \frac{\hat{g}_{\rm eff}^4}{48\pi m_\chi^2}\left(1-\frac{m_{\hat{Z}}^2}{4m_\chi^2}\right)^{-2}\frac{3\hat{T}}{m_\chi}. \tag{46}$$

In this expression $\hat{T}$ is the temperature of the dark sector and we have used the nonrelativistic relation $\langle v^2\rangle = 6\hat{T}/m_\chi$. We emphasize again that $\hat{T}$ is in general no longer equal to the temperature T of the SM gas, because we are allowing for the possibility that the dark sector decouples from the SM well before before the χ particles freeze out.

The relic abundance of χ can be obtained from the Boltzmann equation,

$$\frac{{\rm d}n_\chi}{{\rm d}t} + 3Hn_\chi = -\langle \sigma_{\chi\chi^*\to\hat{\psi}\bar{\hat{\psi}}} v\rangle (n_\chi^2 - (n_\chi^{\rm eq})^2). \tag{47}$$

This can be solved using the methods discussed in Sec. III.

C. Kinetic decoupling between DM and DR

After freeze-out, the system of DM and DR continues to behave as a tightly coupled fluid until kinetic decoupling occurs. This is in analogy to the photon-baryon plasma before recombination, and the DM-SM plasma in the context of the conventional WIMP scenario. Even though DM and DR have chemically decoupled, they are kept in kinetic equilibrium by the elastic scattering of χ with the fermions $\hat{\psi}_i$, which proceeds through an off-shell $\hat{Z}$ in the t-channel. To leading order in the nonrelativistic limit, the cross section for $\chi + \hat{\psi}_i \to \chi + \hat{\psi}_i$ is given by

$$\sigma_{\chi\hat{\psi}_i\to\chi\hat{\psi}_i} = \frac{\hat{g}_Z^4 \hat{q}_\chi^2 \hat{q}_i^2}{2\pi}\frac{E_{\hat{\psi}_i}^2}{m_{\hat{Z}}^4}, \tag{48}$$

where $E_{\hat{\psi}_i}$ represents the energy of the scattering $\hat{\psi}_i$ in the CM frame. Performing a thermal averaging, we obtain

$$\sum_{i=1}^{N_{\hat{\psi}}} n_{\hat{\psi}_i}\langle \sigma_{\chi\hat{\psi}_i\to\chi\hat{\psi}_i} v\rangle = \frac{4\cdot 45\zeta(5)}{4\pi^2}\frac{\hat{g}_{\rm eff}^4}{2\pi}\frac{\hat{T}^5}{m_{\hat{Z}}^4} \equiv \Gamma_{\rm col}, \tag{49}$$

where the overall factor of 4 in front accounts for the two polarizations of $\hat{\psi}$, as well as the contribution from scattering with an anti-$\hat{\psi}_i$. The factor of $45\zeta(5)/4\pi^2$ arises from thermal averaging. Note that $\Gamma_{\rm col}$ represents the rate for a χ to experience a single collision with any one of the $\hat{\psi}_i$. This rate is not, however, the same as the rate for the χ plasma to thermalize with the $\hat{\psi}$ bath. This is because a single collision of a χ particle with a $\hat{\psi}_i$ typically involves a

momentum transfer of only $\mathcal{O}(\hat{T})$, which is not large enough to significantly deflect the direction of the χ, which carries a momentum $\mathcal{O}(\sqrt{m_\chi \hat{T}})$. Viewing the effect of N such collisions as a random walk with N steps, the χ momentum typically changes by $\mathcal{O}(\sqrt{N}\hat{T})$ after N collisions. Requiring that this change be $\mathcal{O}(\sqrt{m_\chi \hat{T}})$, we obtain that $N \sim m_\chi/\hat{T}$. It follows that the rate for the χ plasma to thermalize with the $\hat{\psi}$ bath is given by

$$\frac{\Gamma_{\rm col}}{N} \sim \frac{45\zeta(5)}{\pi^2}\frac{\hat{g}_{\rm eff}^4}{2\pi}\frac{\hat{T}^6}{m_{\hat{Z}}^4 m_\chi}. \tag{50}$$

Then, the temperature $\hat{T}_{\rm D}$ below which the χ plasma thermally decouples from the bath may be estimated as

$$\left.\frac{\Gamma_{\rm col}}{N}\right|_{\hat{T}=\hat{T}_{\rm D}} \sim \left. H \right|_{T=T_{\rm D}}. \tag{51}$$

For the ranges of parameters considered in our benchmark models, a quick estimate tells us that $T_{\rm D} \sim \mathcal{O}(1)$–$\mathcal{O}(10)$ MeV.

Above the kinetic decoupling temperature $T_{\rm D}$, DM is in equilibrium with DR, and they form a tightly coupled fluid. Acoustic oscillations within this fluid have the effect of erasing density perturbations on small scales. As a result, the temperature $T_{\rm D}$ determines the cutoff of the power spectrum, and sets a lower bound on the masses of the smallest halos [74],

$$M_{\rm cut} \simeq 10^5 \left(\frac{T_{\rm D}}{10\ {\rm keV}}\right)^{-3} M_\odot. \tag{52}$$

In principle, this offers a separate way to probe these theories, independent of the CMB. At present, kinetic decoupling temperatures up to about 10 keV can be probed. Unfortunately, in our scenario, $T_{\rm D}$ is too high for the cutoff of short-distance structures to be observable in current experiments.

One possible generalization of our scenario that would lead to observable effects in the DM power spectrum involves allowing the mass $m_{\hat{Z}}$ of the mediator to lie below the weak scale. It is easy to see that the WIMP miracle prediction for DM relic abundance continues to apply, provided the DM candidate itself continues to have weak scale mass and couplings of $\mathcal{O}(1)$ to the mediator. In order to have observable effects, a mediator of mass $\hat{m}_Z \lesssim \mathcal{O}(100)$ MeV would be required. If the mediator mass is further pushed down to $O(\text{MeV})$, exchange of the light $\hat{Z}$ would give rise to sizable DM self-interactions, which can lead to observable effects in the DM power spectrum [75]. The resulting DM scattering cross section is velocity dependent, and can therefore be large enough to resolve small scale structure anomalies while remaining consistent with cosmological bounds, along the lines suggested in [27,76–79]. We leave a detailed study of this possibility for future work.

D. Kinetic decoupling of DM from the SM bath

As we noted earlier, the size of the CMB signals depends on the temperature $T = \hat{T} = T_{\rm kd}$ at which the dark matter sector kinetically decouples from the SM bath. For m_χ in the range between 10 GeV and 100 GeV, the leading processes maintaining the kinetic equilibrium are the elastic scattering of χ off the W, Z, and SM fermions. These processes decouple at different temperatures, and $T_{\rm kd}$ is set by the last process that decouples.

It turns out that at temperatures above ~10 GeV the dominant process is the scattering of DM particles off W bosons. At these temperatures, even if the W bosons are nonrelativistic and their number density begins to be Boltzmann suppressed, it is still more dominant than the competing scattering of χ off a relativistic b quark, as the latter suffers from a small Yukawa coupling. Let us first consider the scattering of a relativistic χ off a nonrelativistic W. The tree-level cross section in this limit is given by

$$\sigma_W = \frac{\kappa^2}{4\pi}\frac{m_W^2}{m_h^4}. \tag{53}$$

Equating the scattering rate $\Gamma_W = n_W \langle \sigma_W v \rangle$ with the Hubble expansion rate H gives an estimate for the temperature at which this process decouples, where n_W represents the equilibrium number density of W bosons, and the relative speed v between the scattering χ and W is unity in the limit under consideration. We thus obtain

$$\begin{aligned} T_{\rm kd} &\sim m_W \left[\log\left(\frac{9\sqrt{10}}{16\pi^4}\frac{M_{\rm P}}{m_h}\frac{m_W^3}{m_h^3}\frac{\kappa^2}{\sqrt{g_*}}\right)\right]^{-1} \\ &= m_W \left[8.5 + \log\left(\frac{\kappa^2}{10^{-10}}\frac{10}{\sqrt{g_*}}\right)\right]^{-1}. \end{aligned} \tag{54}$$

In obtaining this expression, we have assumed that $g_* \gg \hat{g}_*$, so that the energy density is dominated by the SM degrees of freedom. For a similar process with the Z boson rather than the W, every appearance of m_W above should be replaced by m_Z, and the argument of the logarithm is reduced by a factor of 2 because of the fewer degrees of freedom associated with the Z. Therefore, the corresponding decoupling temperature is proportional to m_Z with the same proportionality factor (neglecting the change in the argument of the logarithm), so the Z decouples at a slightly higher temperature than the W.

On the other hand, in the limit where the χ and W are both nonrelativistic, the scattering cross section is given at tree level by

$$\sigma_W = \frac{\kappa^2}{4\pi(m_\chi + m_W)^2}\frac{m_W^4}{m_h^4}. \tag{55}$$

To calculate the rate $n_W\langle\sigma_W v\rangle$, we need to know $\langle v\rangle$. For a single nonrelativistic particle of mass m obeying the Maxwell-Boltzmann distribution with temperature T, an elementary integral gives $\langle v\rangle = \sqrt{8T/(\pi m)}$. We have a two-body system instead, but the relative speed v in the lab frame is the same as that in the CM frame, where the two-body problem reduces to a one-body problem with the reduced mass $\mu_{\chi W} \equiv m_\chi m_W/(m_\chi + m_W)$. We thus have $\langle v\rangle = \sqrt{8T/(\pi\mu_{\chi W})}$. The kinetic decoupling temperature then becomes

$$\begin{aligned} T_{\rm kd} &\sim m_W\left[\log\left(\frac{9\sqrt{5}}{4\pi^{9/2}}\frac{M_{\rm P}}{m_h}\frac{m_W^3}{m_h^3}\frac{\mu_{\chi W}^2}{m_\chi^2}\sqrt{\frac{m_W}{\mu_{\chi W}}}\frac{\kappa^2}{\sqrt{g_*}}\right)\right]^{-1} \\ &= m_W\left[8.9 + \log\left(\frac{\mu_{\chi W}^2}{m_\chi^2}\sqrt{\frac{m_W}{\mu_{\chi W}}}\frac{\kappa^2}{10^{-10}}\frac{10}{\sqrt{g_*}}\right)\right]^{-1}. \end{aligned} \tag{56}$$

At temperatures below ~10 GeV, scattering of DM off SM fermions becomes increasingly important, and eventually dominates. At these temperatures the DM particle χ is nonrelativistic, while the SM fermions may be relativistic or nonrelativistic. In the case where the scattering SM fermion f is relativistic, the tree-level cross section is given by

$$\sigma_f = \frac{\kappa^2}{8\pi m_\chi^2}\frac{m_f^2 p^2}{m_h^4}, \tag{57}$$

where p is the magnitude of the 3-momenta of the scattering particles in the CM frame, and higher order terms in p/m_χ have been neglected. In this leading nonrelativistic approximation, the thermal average $\langle p^2\rangle$ in the CM frame is the same as that in the lab frame, as the difference between the two frames itself is an $\mathcal{O}(p/m_\chi)$ effect. Therefore, we evaluate $\langle p^2\rangle$ and the number density n_f simply in the lab frame in the standard way, obtaining

$$\langle p^2\rangle = \frac{15\zeta(5)}{\zeta(3)}T^2, \qquad n_f = 4N_{\rm c}\cdot\frac{3\zeta(3)}{4\pi^2}T^3, \tag{58}$$

where $N_{\rm c}$ is the number of colors carried by the fermion species f. Notice, however, that the relevant reaction rate to maintain a kinetic equilibrium is not simply given by $n_f\langle\sigma_f v\rangle$, because a single collision of a heavy particle χ with a relativistic particle f with $p \ll m_\chi$ hardly changes the direction of the χ momentum. Since the χ momentum is on average of order $\sqrt{m_\chi T}$, and a typical momentum transfer via a single collision is of order $p \sim T$, the number of collisions N required to alter the χ momentum by an $\mathcal{O}(1)$ fraction is given by $\sqrt{N}T \sim \sqrt{m_\chi T}$, i.e., $N \sim m_\chi/T$. The relevant reaction rate to maintain a kinetic equilibrium, therefore, is given by $\Gamma_f = n_f\langle\sigma_f v\rangle/N$. Then, from $\Gamma_f \sim H$, we obtain an estimate for the kinetic decoupling temperature:

$$\begin{aligned} T_{\rm kd} &\sim m_h\left(\frac{16\pi^{9/2}}{135\sqrt{5}\zeta(5)}\frac{1}{N_{\rm c}}\frac{m_\chi^3}{m_f^2 M_{\rm P}}\frac{\sqrt{g_*}}{\kappa^2}\right)^{\frac{1}{4}} \\ &\sim 4.3\ \text{GeV}\times\left(\frac{3}{N_{\rm c}}\frac{m_\chi^3}{(10\ \text{GeV})^3}\frac{m_b^2}{m_f^2}\frac{10^{-10}}{\kappa^2}\frac{\sqrt{g_*}}{10}\right)^{\frac{1}{4}}, \end{aligned} \tag{59}$$

where m_b is the b-quark mass.

If the SM fermion is also nonrelativistic, the tree-level cross section in the leading nonrelativistic approximation is given by

$$\sigma_f = \frac{\kappa^2}{4\pi(m_\chi + m_f)^2}\frac{m_f^4}{m_h^4}. \tag{60}$$

For thermal averaging, we use $\langle v\rangle = \sqrt{8T/(\pi\mu_{\chi f})}$, similarly to what we did below Eq. (55). Furthermore, the number of collisions N required to randomize the motion of χ is given by $\sqrt{N}\sqrt{m_f T} \sim \sqrt{m_\chi T}$, i.e., $N \sim m_\chi/m_f$. Then, from $n_f\langle\sigma_f v\rangle/N \sim H$, we obtain

$$\begin{aligned} T_{\rm kd} &\sim m_f\left[\log\left(\frac{3\sqrt{5}}{2\pi^{9/2}}\cdot N_{\rm c}\cdot\frac{M_{\rm P}}{m_h}\frac{m_f^6}{m_h^3 m_\chi^3}\left(\frac{\mu_{\chi f}}{m_f}\right)^{\frac{3}{2}}\frac{\kappa^2}{\sqrt{g_*}}\right)\right]^{-1} \\ &= m_f\left[5.2 + \log\left(N_{\rm c}\left(\frac{100 m_f^2}{m_h m_\chi}\right)^3\left(\frac{\mu_{\chi f}}{m_f}\right)^{\frac{3}{2}}\frac{\kappa^2}{10^{-6}}\frac{10}{\sqrt{g_*}}\right)\right]^{-1}. \end{aligned} \tag{61}$$

Note that the "reference value" of κ used here is 10^{-3}, which differs from Eqs. (54), (56), and (59), where the value used was 10^{-5}. This reflects the fact that this process is relevant only if κ is sufficiently large, even for the b quark.

In Fig. 4, we plot the kinetic decoupling temperature against the dark matter mass, for several different values of the coupling κ. We see that for the range of values of κ that can be probed in current and future collider experiments, the kinetic decoupling temperature lies below several GeV and above several hundred MeV. In particular, the kinetic decoupling occurs before a drastic change in the number of relativistic SM degrees of freedom due to QCD phase transition.

E. Signals

Given the dark matter mass and the value of the coupling constant κ, we can determine the temperature $T_{\rm kd}$ at which the dark sector kinetically decouples from the SM. We can then use Eq. (3) to obtain $\Delta N_{\rm eff}$ and Eq. (12) to obtain the angular shifts of the CMB peaks. In our benchmark model, $\hat{g}_*$ and $\hat{g}_{*\rm kd}$ are given by

$$\hat{g}_* = 2 + \frac{7}{2}N_{\hat{\psi}}, \qquad \hat{g}_{*\rm kd} = n + \frac{7}{2}N_{\hat{\psi}}. \tag{62}$$

We assume that the $\hat{Z}$ boson is already nonrelativistic when the SM and hidden sectors decouple. Then $n = 2$ if the DM

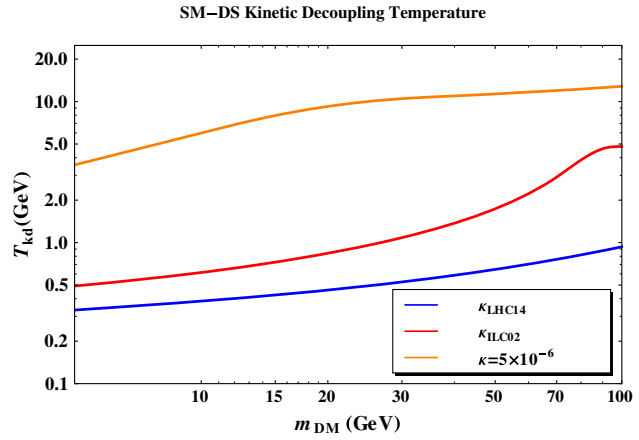

FIG. 4 (color online). The kinetic decoupling temperature $T_{\rm kd}$ between the SM and hidden sectors as a function of the DM mass $m_{\rm DM}$ for three values of κ: $\kappa_{\rm LHC14} = 7 \times 10^{-3}, \kappa_{\rm ILC02} = 9.5 \times 10^{-4}$ and $\kappa = 5 \times 10^{-6}$.

candidate is already nonrelativistic when the SM and dark sectors decouple, and $n = 4$ otherwise.

The results for $N_{\hat{\psi}} = 1$ are shown in the upper panel of Fig. 5 for three different values of κ. The smallest of the values studied, $\kappa = 5 \times 10^{-6}$, corresponds to the minimum

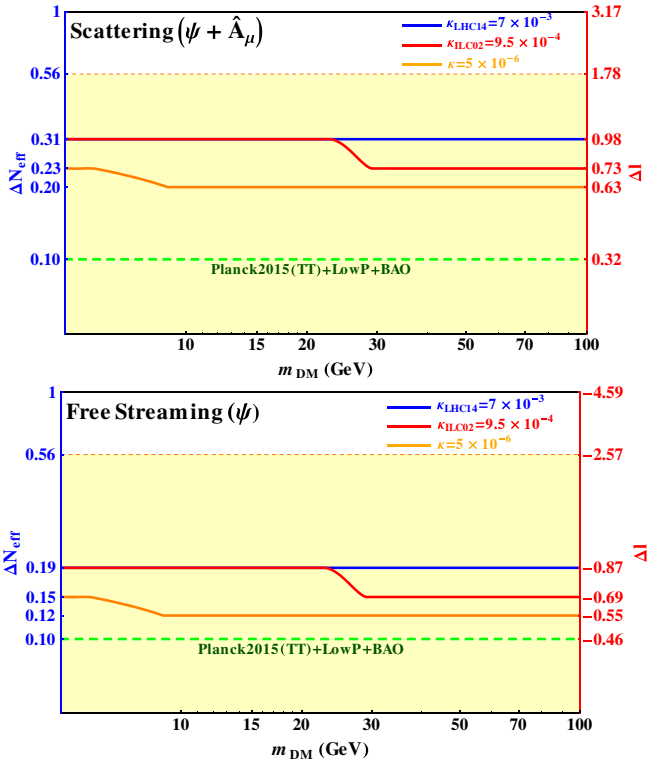

FIG. 5 (color online). $\Delta N_{\rm eff}$ and $\Delta\ell$ as a function of $m_{\rm DM}$. It is assumed that $M_{\hat{Z}} > m_{\rm DM}$. Three values of κ are considered: $\kappa_{\rm LHC14}, \kappa_{\rm ILC02}$ and $\kappa = 5 \times 10^{-6}$. Also shown are the 2015 Planck results: the central value (green dashed line) and the 2σ constraint (orange dashed line).

value of κ that can ensure that the SM and hidden sector are in thermal equilibrium at or above the weak scale. The other two values studied correspond to the limits that can be placed on κ at the LHC and at a lepton collider. In the figure we have plotted the current limits on $\Delta N_{\rm eff}$ from the Planck experiment. Although in the region of light DM masses that may be probed at the 14 TeV LHC the predicted $\Delta N_{\rm eff}$ are above the central value from Planck data fit, they are still well within 95% C.L., and are large enough to be detected in upcoming experiments. It is also important to note that these bounds are not immediately applicable to this model since in the standard Planck analysis, it is assumed that the contribution to $\Delta N_{\rm eff}$ is free streaming. A fresh analysis that relaxes this assumption by including scattering radiation is required to determine the current limits on this scenario.

We see from Fig. 5 that $\Delta N_{\rm eff} \gtrsim 0.2$ in this class of models for the entire range of DM masses. Then, based on the discussion in Sec. II we expect that upcoming experiments will offer the possibility of distinguishing this scenario from one where $\Delta N_{\rm eff}$ is the same, but the DR free streams. For the purposes of comparison, in the lower panel of Fig. 5 we have plotted $\Delta N_{\rm eff}$ and $\Delta\ell$ for the same model, but without the U(1) gauge symmetry. The DR now consists of only one massless fermion species $\hat{\psi}$. Since the gauge boson $\hat{A}_\mu$ is now absent, the DR free streams rather than scatters. We see from the figure that although the magnitudes of $\Delta N_{\rm eff}$ and $\Delta\ell$ are comparable in size to the benchmark model, the sign of $\Delta\ell$ is opposite in sign. It is this difference that we expect will help distinguish between free streaming and scattering DR

V. CONCLUSIONS

In this paper, we have explored a scenario where the DM candidate is part of a hidden sector whose particles carry no charges under the SM gauge groups, and whose couplings to the SM states, though present, are small. The abundance of DM is assumed to be determined primarily by annihilation to massless states that lie within the hidden sector. Then, if we further assume that the weak scale is the only mass scale in the hidden sector, so that the mass of the DM particle and its annihilation cross section are both set by this scale, the observed abundance of DM can be naturally explained. This framework is motivated by an alternative realization of thermal WIMP DM paradigm that is naturally compatible with limits from direct, indirect and collider searches for DM thus far.

A robust consequence of this framework is the existence of DR, associated with the massless states in the hidden sector. The contribution of this DR to the energy density of the universe during the era of recombination epoch manifests itself observationally as a contribution to the effective number of neutrino species, $\Delta N_{\rm eff}$. In addition, massless particles constituting DR may or may not interact with one another. We determined the shift in the locations of the

CMB peaks, $\Delta\ell$, as a function of the number of free streaming DR species, $\Delta N_{\rm eff}^{\rm free}$, and scattering species, $\Delta N_{\rm eff}^{\rm scatt}$. We found that free streaming and scattering species shift the peaks in opposite directions, so that by combining this effect with the measurement of the total $\Delta N_{\rm eff}$ mentioned above, we can separately determine $\Delta N_{\rm eff}^{\rm free}$ and $\Delta N_{\rm eff}^{\rm scatt}$. We also calculated the corrections to the amplitudes of the scalar and tensor modes of the CMB arising from the presence of DR, and showed that the sign of the correction depends on whether the DR scatters or free streams.

We have found that provided the hidden sector is initially in thermal equilibrium with the SM degrees of freedom at temperatures at or above the weak scale, there is a robust prediction for a lower bound on $\Delta N_{\rm eff}$ of about 0.02. This is large enough to be observed by future CMB Stage-IV experiments. In the scenario where the DR has self-interactions, assuming naturalness, $\Delta N_{\rm eff}$ is expected to lie well above this lower bound, making it large enough to be observed in upcoming experiments such as CMBPol. We further constructed a simple model that realizes this scenario. In our model, the SM and hidden sector are initially kept in thermal equilibrium through the Higgs portal. We have determined the size of the $\Delta N_{\rm eff}$ signal, and have shown that it is large enough to be detected in upcoming experiments. These experiments are also expected to be sensitive enough to the $\Delta\ell$ signal to allow the possibility of distinguishing between free streaming DR and scattering DRİn addition, we find that there are regions of parameter space where invisible decays of the Higgs into hidden sector states can be used to probe this model at colliders.

An important point to reiterate is that the bounds on $\Delta N_{\rm eff}$ derived from the standard analyses, such as by Planck, may not be directly applicable to our scenario where the DR may be self-scattering. A dedicated analysis parametrized by $\Delta N_{\rm eff}^{\rm free}$ and $\Delta N_{\rm eff}^{\rm scatt}$ instead of a single $\Delta N_{\rm eff}$ is required to determine the exact limits on this scenario.

The general possibility that dark matter may arise from a sector hidden from the visible matter of the SM has drawn considerable interest recently, due in no small part to the increasing experimental limits on the conventional WIMP DM paradigm. Our work highlights that in this scenario which is challenging or perhaps even impossible for conventional DM searches, CMB experiments may be able to shed light on the nature of the DM sector, which is worthy of further exploration.

ACKNOWLEDGMENTS

We thank Chris Brust for helpful discussions. Z. C., Y. C. and S. H. are supported by the NSF under Grant No. PHY-1315155 and the Maryland Center for Fundamental Physics. Y. C. is also supported by Perimeter Institute for Theoretical Physics, which is supported by the Government of Canada through Industry Canada and by the Province of Ontario through the Ministry of Research and Innovation. S. H. is also supported in part by a fellowship from The Kwanjeong Educational Foundation. T. O. is supported by the DOE under Grant No. DE-FG02-13ER41942.

Note added.—While we were completing this paper, we received [80], which overlaps with some of the ideas presented here.

[1] P. A. R. Ade *et al.* (Planck Collaboration), Planck 2015 results. XIII. Cosmological parameters, arXiv:1502.01589.
[2] B. W. Lee and S. Weinberg, Cosmological Lower Bound on Heavy Neutrino Masses, Phys. Rev. Lett. **39**, 165 (1977).
[3] M. I. Vysotsky, A. D. Dolgov, and Y. B. Zeldovich, Cosmological restriction on neutral lepton masses, Pis'ma Zh. Eksp. Teor. Fiz. **26**, 200 (1977) [JETP Lett. **26**, 188 (1977)].
[4] E. Aprile *et al.* (XENON100 Collaboration), Dark Matter Results from 225 Live Days of XENON100 Data, Phys. Rev. Lett. **109**, 181301 (2012).
[5] D. S. Akerib *et al.* (LUX Collaboration), First Results from the LUX Dark Matter Experiment at the Stanford Underground Research Facility, Phys. Rev. Lett. **112**, 091303 (2014).
[6] M. Ackermann *et al.* (Fermi-LAT Collaboration), Dark matter constraints from observations of 25 Milky Way satellite galaxies with the Fermi Large Area Telescope, Phys. Rev. D **89**, 042001 (2014).
[7] A. A. Abdo *et al.* (Fermi-LAT Collaboration), Observations of Milky Way Dwarf Spheroidal galaxies with the Fermi-LAT detector and constraints on dark matter models, Astrophys. J. **712**, 147 (2010).
[8] A. Djouadi, O. Lebedev, Y. Mambrini, and J. Quevillon, Implications of LHC searches for Higgs–portal dark matter, Phys. Lett. B **709**, 65 (2012).
[9] D. Tucker-Smith and N. Weiner, Inelastic dark matter, Phys. Rev. D **64**, 043502 (2001).
[10] Y. Cui, D. E. Morrissey, D. Poland, and L. Randall, Candidates for inelastic dark matter, J. High Energy Phys. 05 (2009) 076.
[11] L. M. Krauss, S. Nasri, and M. Trodden, A model for neutrino masses and dark matter, Phys. Rev. D **67**, 085002 (2003).

[12] E. A. Baltz and L. Bergstrom, Detection of leptonic dark matter, Phys. Rev. D **67**, 043516 (2003).
[13] J. Kopp, V. Niro, T. Schwetz, and J. Zupan, DAMA/LIBRA and leptonically interacting dark matter, Phys. Rev. D **80**, 083502 (2009).
[14] K. Cheung, K. Mawatari, E. Senaha, P. Y. Tseng, and T. C. Yuan, The top window for dark matter, J. High Energy Phys. 10 (2010) 081.
[15] P. Agrawal, S. Blanchet, Z. Chacko, and C. Kilic, Flavored dark matter, and its implications for direct detection and colliders, Phys. Rev. D **86**, 055002 (2012).
[16] Y. Zhang, Top quark mediated dark matter, Phys. Lett. B **720**, 137 (2013).
[17] A. Kumar and S. Tulin, Top-flavored dark matter and the forward-backward asymmetry, Phys. Rev. D **87**, 095006 (2013).
[18] C. Kilic, M. D. Klimek, and J. H. Yu, Signatures of top flavored dark matter, Phys. Rev. D **91**, 054036 (2015).
[19] D. P. Finkbeiner and N. Weiner, Exciting dark matter and the INTEGRAL/SPI 511 keV signal, Phys. Rev. D **76**, 083519 (2007).
[20] M. Pospelov, A. Ritz, and M. B. Voloshin, Secluded WIMP dark matter, Phys. Lett. B **662**, 53 (2008).
[21] J. L. Feng and J. Kumar, The WIMPless Miracle: Dark-Matter Particles without Weak-Scale Masses or Weak Interactions, Phys. Rev. Lett. **101**, 231301 (2008).
[22] J. L. Feng, H. Tu, and H. B. Yu, Thermal relics in hidden sectors, J. Cosmol. Astropart. Phys. 10 (2008) 043.
[23] I. Cholis, L. Goodenough, and N. Weiner, High energy positrons and the WMAP haze from exciting dark matter, Phys. Rev. D **79**, 123505 (2009).
[24] K. Agashe, Y. Cui, L. Necib, and J. Thaler, (In)direct detection of boosted dark matter, J. Cosmol. Astropart. Phys. 10 (2014) 062.
[25] J. Berger, Y. Cui, and Y. Zhao, Detecting boosted dark matter from the sun with large volume neutrino detectors, J. Cosmol. Astropart. Phys. 02 (2015) 005.
[26] L. Ackerman, M. R. Buckley, S. M. Carroll, and M. Kamionkowski, Dark matter and dark radiation, Phys. Rev. D **79**, 023519 (2009).
[27] J. L. Feng, M. Kaplinghat, H. Tu, and H. B. Yu, Hidden charged dark matter, J. Cosmol. Astropart. Phys. 07 (2009) 004.
[28] U. Frana, R. A. Lineros, J. Palacio, and S. Pastor, Probing interactions within the dark matter sector via extra radiation contributions, Phys. Rev. D **87**, 123521 (2013).
[29] S. Weinberg, Goldstone Bosons as Fractional Cosmic Neutrinos, Phys. Rev. Lett. **110**, 241301 (2013).
[30] C. Garcia-Cely, A. Ibarra, and E. Molinaro, Dark matter production from Goldstone boson interactions and implications for direct searches and dark radiation, J. Cosmol. Astropart. Phys. 11 (2013) 061.
[31] C. Garcia-Cely, A. Ibarra, and E. Molinaro, Cosmological and astrophysical signatures of dark matter annihilations, J. Cosmol. Astropart. Phys. 02 (2014) 032.
[32] M. Blennow, E. Fernandez-Martinez, O. Mena, J. Redondo, and P. Serra, Asymmetric dark matter and dark radiation, J. Cosmol. Astropart. Phys. 07 (2012) 022.
[33] R. Diamanti, E. Giusarma, O. Mena, M. Archidiacono, and A. Melchiorri, Dark radiation and interacting scenarios, Phys. Rev. D **87**, 063509 (2013).
[34] R. Foot and S. Vagnozzi, Dissipative hidden sector dark matter, Phys. Rev. D **91**, 023512 (2015).
[35] R. Foot and S. Vagnozzi, Diurnal modulation signal from dissipative hidden sector dark matter, Phys. Lett. B **748**, 61 (2015).
[36] K. Nakayama, F. Takahashi, and T. T. Yanagida, A theory of extra radiation in the Universe, Phys. Lett. B **697**, 275 (2011).
[37] W. Fischler and J. Meyers, Dark radiation emerging after big bang nucleosynthesis?, Phys. Rev. D **83**, 063520 (2011).
[38] K. S. Jeong and F. Takahashi, Self-interacting dark radiation, Phys. Lett. B **725**, 134 (2013).
[39] S. Galli, M. Martinelli, A. Melchiorri, L. Pagano, B. D. Sherwin, and D. N. Spergel, Constraining fundamental physics with future CMB experiments, Phys. Rev. D **82**, 123504 (2010).
[40] K. N. Abazajian *et al.* (Topical Conveners: K. N. Abazajian, J. E. Carlstrom, A. T. Lee Collaboration), Neutrino physics from the cosmic microwave background and large scale structure, Astropart. Phys. **63**, 66 (2015).
[41] P. J. E. Peebles, The role of neutrinos in the evolution of primeval adiabatic perturbations, Astrophys. J. **180**, 1 (1973).
[42] W. Hu and N. Sugiyama, Small scale cosmological perturbations: An analytic approach, Astrophys. J. **471**, 542 (1996).
[43] S. Bashinsky and U. Seljak, Neutrino perturbations in CMB anisotropy and matter clustering, Phys. Rev. D **69**, 083002 (2004).
[44] S. Weinberg, Damping of tensor modes in cosmology, Phys. Rev. D **69**, 023503 (2004).
[45] R. Flauger and S. Weinberg, Tensor microwave background fluctuations for large multipole order, Phys. Rev. D **75**, 123505 (2007).
[46] Z. Chacko, L. J. Hall, T. Okui, and S. J. Oliver, CMB signals of neutrino mass generation, Phys. Rev. D **70**, 085008 (2004).
[47] Z. Chacko, L. J. Hall, S. J. Oliver, and M. Perelstein, Late Time Neutrino Masses, the LSND Experiment and the Cosmic Microwave Background, Phys. Rev. Lett. **94**, 111801 (2005).
[48] T. Okui, Searching for composite neutrinos in the cosmic microwave background, J. High Energy Phys. 09 (2005) 017.
[49] J. F. Beacom, N. F. Bell, and S. Dodelson, Neutrinoless Universe, Phys. Rev. Lett. **93**, 121302 (2004).
[50] S. Hannestad, Structure formation with strongly interacting neutrinos—Implications for the cosmological neutrino mass bound, J. Cosmol. Astropart. Phys. 02 (2005) 011.
[51] R. Trotta and A. Melchiorri, Indication for Primordial Anisotropies in the Neutrino Background from WMAP and SDSS, Phys. Rev. Lett. **95**, 011305 (2005).
[52] N. F. Bell, E. Pierpaoli, and K. Sigurdson, Cosmological signatures of interacting neutrinos, Phys. Rev. D **73**, 063523 (2006).

[53] M. Cirelli and A. Strumia, Cosmology of neutrinos and extra light particles after WMAP3, J. Cosmol. Astropart. Phys. 12 (2006) 013.
[54] A. Friedland, K. M. Zurek, and S. Bashinsky, Constraining models of neutrino mass and neutrino interactions with the Planck satellite, arXiv:0704.3271.
[55] M. Archidiacono and S. Hannestad, Updated constraints on non-standard neutrino interactions from Planck, J. Cosmol. Astropart. Phys. 07 (2014) 046.
[56] F. Forastieri, M. Lattanzi, and P. Natoli, Constraints on secret neutrino interactions after Planck, arXiv:1504.04999.
[57] Z. Hou, R. Keisler, L. Knox, M. Millea, and C. Reichardt, How massless neutrinos affect the cosmic microwave background damping tail, Phys. Rev. D **87**, 083008 (2013).
[58] C. Brust, D. E. Kaplan, and M. T. Walters, New light species and the CMB, J. High Energy Phys. 12 (2013) 058.
[59] D. A. Dicus and W. W. Repko, Comment on damping of tensor modes in cosmology, Phys. Rev. D **72**, 088302 (2005).
[60] B. A. Stefanek and W. W. Repko, Analytic description of the damping of gravitational waves by free streaming neutrinos, Phys. Rev. D **88**, 083536 (2013).
[61] R. Jinno, T. Moroi, and K. Nakayama, Probing dark radiation with inflationary gravitational waves, Phys. Rev. D **86**, 123502 (2012).
[62] E. W. Kolb and M. S. Turner, The early universe, Front. Phys. **69**, 1 (1990).
[63] M. Srednicki, R. Watkins, and K. A. Olive, Calculations of relic densities in the early universe, Nucl. Phys. **B310**, 693 (1988).
[64] P. Gondolo and G. Gelmini, Cosmic abundances of stable particles: Improved analysis, Nucl. Phys. **B360**, 145 (1991).
[65] (ATLAS Collaboration), Reports No. ATLAS-CONF-2015-004, No. ATLAS-COM-CONF-2015-004.
[66] (CMS Collaboration), Report No. CMS-PAS-HIG-14-038.
[67] G. Aad *et al.* (ATLAS Collaboration), Search for Invisible Decays of a Higgs Boson Produced in Association with a Z Boson in ATLAS, Phys. Rev. Lett. **112**, 201802 (2014).
[68] S. Chatrchyan *et al.* (CMS Collaboration), Search for invisible decays of Higgs bosons in the vector boson fusion and associated ZH production modes, Eur. Phys. J. C **74**, 2980 (2014).
[69] (ATLAS Collaboration), Physics at a high-luminosity LHC with ATLAS, arXiv:1307.7292.
[70] (CMS Collaboration), Projected performance of an upgraded CMS detector at the LHC and HL-LHC: Contribution to the Snowmass process, arXiv:1307.7135.
[71] S. Dawson, A. Gritsan, H. Logan, J. Qian, C. Tully, R. Van Kooten, A. Ajaib, A. Anastassov *et al.*, Higgs working group report of the Snowmass 2013 community planning study, arXiv:1310.8361.
[72] Z. Chacko, Y. Cui, and S. Hong, Exploring a dark sector through the Higgs portal at a lepton collider, Phys. Lett. B **732**, 75 (2014).
[73] T. Han, Z. Liu, and J. Sayre, Potential precision on Higgs couplings and total width at the ILC, Phys. Rev. D **89**, 113006 (2014).
[74] A. Loeb and M. Zaldarriaga, The small-scale power spectrum of cold dark matter, Phys. Rev. D **71**, 103520 (2005).
[75] D. N. Spergel and P. J. Steinhardt, Observational Evidence for Self-Interacting Cold Dark Matter, Phys. Rev. Lett. **84**, 3760 (2000).
[76] A. Loeb and N. Weiner, Cores in Dwarf Galaxies from Dark Matter with a Yukawa Potential, Phys. Rev. Lett. **106**, 171302 (2011).
[77] L. G. van den Aarssen, T. Bringmann, and C. Pfrommer, Is Dark Matter with Long-Range Interactions a Solution to All Small-Scale Problems of ΛCDM Cosmology?, Phys. Rev. Lett. **109**, 231301 (2012).
[78] S. Tulin, H. B. Yu, and K. M. Zurek, Resonant Dark Forces and Small Scale Structure, Phys. Rev. Lett. **110**, 111301 (2013).
[79] S. Tulin, H. B. Yu, and K. M. Zurek, Beyond collisionless dark matter: Particle physics dynamics for dark matter halo structure, Phys. Rev. D **87**, 115007 (2013).
[80] M. A. Buen-Abad, G. Marques-Tavares, and M. Schmaltz, Non-Abelian dark matter and dark radiation, Phys. Rev. D **92**, 023531 (2015).